Journal of Materials Chemistry C

PAPER

View Article Online
View Journal | View Issue

Cite this: J. Mater. Chem. C, 2015, 3, 2933

Core–shell CdS:Ga–ZnTe:Sb p–n nano-heterojunctions: fabrication and optoelectronic characteristics

Li Wang,*[ab] Hong-Wei Song,[a] Zhen-Xing Liu,[a] Xu Ma,[a] Ran Chen,[a] Yong-Qiang Yu,[a] Chun-Yan Wu,[a] Ji-Gang Hu,[a] Yan Zhang,[a] Qiang Li[a] and Lin-Bao Luo*[a]

Received 23rd December 2014,
Accepted 1st February 2015

DOI: 10.1039/c4tc02943g

www.rsc.org/MaterialsC

In this study, we reported on the construction of p–n junctions based on crystalline Ga-doped CdS–polycrystalline ZnTe nanostructures (NSs) for optoelectronic device application. The coaxial nano-heterojunction was fabricated by a two-step growth method. It is found that the absorption edge of CdS:Ga–ZnTe:Sb core–shell NSs red shifted to about 580 nm, compared with CdS nanowires (520 nm). The as-fabricated core–shell p–n junction exhibited obvious rectification characteristics with a low turn-on voltage of ~0.25 V. What is more, it showed stable and repeatable photoresponse to 638 nm light illumination, with a responsivity and a detectivity of 1.55×10^3 A W^{-1} and 8.7×10^{13} cm $Hz^{1/2}$ W^{-1}, respectively, much higher than other photodetectors with similar device configurations. The generality of this study suggests that the present coaxial CdS:Ga–ZnTe:Sb core–shell nano-heterojunction will have great potential applications in future nano-optoelectronic devices.

Introduction

One-dimensional semiconductor nanostructures (NSs) including nanotubes (NTs), nanowires (NWs), and nanorods (NRs), are technologically significant as they are emerging as attractive building blocks for the assembly of electronic and optoelectronic devices owing to their novel electrical, magnetic, and optical properties, which differ from their corresponding bulk and thin film counterparts.[1–3] Coaxial p–n nanostructures as some of the most fundamental building blocks have been of particular interest in that their properties can be easily tailored by changing the diameter and the chemical composition of both the core and the shell. In addition, compared with other geometries, core–shell p–n structure exhibits unique advantages in terms of increased surface, shortened carrier collection path length and reduced reflection, which are vitally important for high-performance electronic and opto-electronic devices at the nanoscale level.[4–6] So far a number of approaches have been developed to fabricate coaxial core–shell p–n nanostructures, including SA-MOVPE (selective area metal–organic vapor phase epitaxy),[7] SILAR (successive ion layer adsorption and reaction),[8] CVD (chemical vapor deposition),[9] and ALD (atomic layer deposition).[10] Based on these p–n core–shell semiconductor nanostructures, a variety of nanodevices (*e.g.*, nanogenerators,[11] photovoltaic devices,[12,13] lithium batteries,[14,15] *etc.*) with high performance have been fabricated.

Among the various II–VI group semiconductor (*e.g.*, CdS, CdSe, ZnS, ZnSe *etc.*) materials,[16,17] cadmium sulfide (CdS, band-gap: 2.4 eV) has been widely investigated. To date, a number of one-dimensional CdS nanostructures (*e.g.*, NW and NR) have demonstrated potential application in water splitting,[18] field effect transistors (FETs),[19,20] solar cells,[21,22] lasers,[23,24] waveguides,[25] logic circuits,[26] and visible light photodetectors.[27,28] In spite of this progress, there are few studies dealing with the fabrication of CdS core–shell p–n junctions. This scarcity is mainly due to the unavailability of p-type doping of CdS NSs. Thermodynamic studies have revealed that CdS can only exist as an n-type conductor in thermodynamic equilibrium as a result of the strong self-compensation effect, deep acceptor level and low solubility of dopants.[29] A similar phenomenon is also observed on zinc telluride (ZnTe), which is naturally p-type doping.[30] In fact, due to such a difficulty in doping, it is highly challenging to fabricate CdS or ZnTe nanostructures based on p–n junctions. In this paper, we present a systematic study on the fabrication of Ga-doped CdS–Sb-doped ZnTe core–shell hetero-junctions for optoelectronic device application *via* a simple and flexible CVD method. The core–shell p–n junction devices exhibit excellent rectifying characteristics with a low turn on voltage of ~0.25 V, a rectification ratio of ~10^2, and an

[a] School of Electronic Science and Applied Physics and Anhui Provincial Key Laboratory of Advanced Materials and Devices, Hefei University of Technology, Hefei, Anhui 230009, People's Republic of China. E-mail: wlhgd@hfut.edu.cn, luolb@hfut.edu.cn

[b] Department of Materials Science and Engineering, University of Toronto, Toronto, Ontario M5S 3E4, Canada

ideality factor of 1.28. Moreover, the p–n nano-heterojunction exhibits typical sensitivity to 638 nm irradiation, with an I_{light}/I_{dark} ratio of 20. The responsivity and detectivity are estimated to be 1.55×10^3 A W^{-1} and 8.7×10^{12} cm $Hz^{1/2}$ W^{-1}, respectively, much higher than other photodetectors with similar configurations. It is expected that the present CdS:Ga–ZnTe:Sb NSs will have great potential for application in optoelectronic devices.

Experimental details

Synthesis and structural analysis of the nano-heterojunction

The synthesis of CdS:Ga–ZnTe:Sb core–shell coaxial NSs was conducted in a horizontal tube furnace *via* a two-step vapor growth process. The gallium doped CdS NWs were synthesized as the core at first. Briefly, ~0.5 g of mixed powder consisting of CdS (Aladdin, purity 99.999%), Ga (Sinopharm Chemical reagent, purity 99.999%) and Ga_2O_3 (Sinopharm Chemical reagent, purity 99.999%) was used as the evaporation source and placed at the central region of the tube furnace. The molar ratio of Ga and Ga_2O_3 was set to be 4 : 1 to allow the generation of Ga vapor during the reaction process. What is more, the mass ratio of the Ga and Ga_2O_3 mixture to CdS was found to be ~8% to ensure sufficient doping content. Si substrates coated with 10 nm of the gold catalyst were then placed in the downstream position about 10 cm from the evaporation source. After evacuating to a base pressure of 5×10^{-3} Pa, Ar (5% H_2 in volume) gas was used as the carrier gas with a constant flow ratio of 30 sccm (standard-state cubic centimeter per minute). The furnace was heated up to 930 °C at a rate of 21 °C min^{-1}, and maintained at this temperature for 1.5 h under a pressure of 160 Torr. After the furnace was cooled naturally down to room temperature, bright-yellow colored wool-like CdS:Ga NWs were deposited on the Si substrates. The ZnTe shell doped with Sb was deposited through co-evaporation of Sb and ZnTe. The powder of Sb (Sinopharm Chemical reagent, purity 99.999%) and ZnTe (Xiya reagent, purity 99.99%) in a mass ratio of 1 : 8 was loaded into two separate alumina boats and transferred to the upstream and center regions of the furnace with distances of 6 and 14 cm, respectively. The as-synthesized CdS:GaNWs were then placed at the downstream position, ~10 cm away from the ZnTe source. The furnace was then heated to 880 °C and maintained at this temperature for 1 h. During growth, a constant Ar (5% H_2 in volume) gas flow of 30 sccm was fed and the pressure in the tube was kept at 10 Torr. The structure and morphology of the as-synthesized product were characterized by X-ray diffraction (XRD, D/MAX2500V, with Cu-Kα radiation), field-emission scanning electron microscopy (FESEM, SU8020), and high-resolution transmission electron microscopy (HRTEM, JEM-2100F). The composition of the product was detected by energy-dispersive X-ray spectroscopy (EDX attached to the SEM) and X-ray photoelectron spectroscopy (XPS, Thermo ESCSLAB 250). The absorption spectra were recorded using an AA800 spectrophotometer.

Fabrication and analysis of the p–n nano-heterojunction device

To fabricate the p–n hetero-junction device, the as-synthesized CdS:Ga–ZnTe:Sb NSs were uniformly dispersed on SiO_2(300 nm)/p^+-Si substrates at first. Source and drain electrodes for the outer ZnTe:Sb shell were defined by photolithography and subsequently Cu (5 nm)\Au (45 nm) double-layer electrodes were deposited in a high-vacuum e-beam system. Afterwards, additional photolithography and wet etching in diluted HCl solution (volume ratio of 1 : 1.5) at room temperature were performed to expose the CdS:Ga core by removing the ZnTe:Sb shell. Eventually, the In electrodes were fabricated on the top of the exposed CdS:Ga core *via* photolithography and e-beam evaporation. To assess the electrical properties of the ZnTe:Sb shells and CdS:Ga cores, nano-FETs based on the single CdS:GaNW and ZnTe:Sb shells were constructed. The electrical measurements were

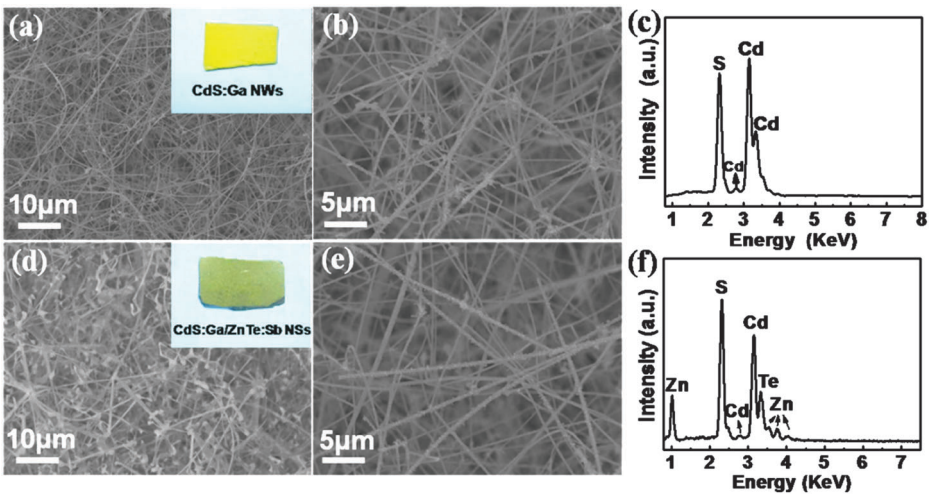

Fig. 1 (a) FESEM image of CdS:Ga NWs; the inset shows the optical picture. (b) FESEM image of CdS:GaN Ws at large magnifications. (c) EDS analysis of CdS:Ga NWs. (d) FESEM image of CdS:Ga–ZnTe:Sb core–shell NSs; the inset shows the optical picture. (e) FESEM image of the NSs at large magnification. (f) EDS analysis of CdS:Ga–ZnTe:Sb core–shell NSs.

carried out at room temperature by using a semiconductor *I–V* characterization system (4200-SCS, Keithley Co.).

Results and discussion

After synthesis, both bright-yellow CdS:GaNWs and dark-yellow core–shell CdS:Ga–ZnTe:Sb NSs (see Fig. 1(a)) were directly transferred into a SEM chamber for morphology study. The FESEM images show the morphology of the CdS:Ga–ZnTe:Sb core–shell nanostructures changed obviously compared with the pristine CdS:Ga NWs (Fig. 1(a) and (d)). It is noted that the surface of NWs is smooth and the size is uniform along the NWs' entire length, with a diameter of 200–300 nm and a typical length of 20–40 μm, respectively. Notably, the morphology of NWs is well retained after deposition with the ZnTe shell (Fig. 1(d)). The energy dispersive spectroscopy (EDS) analysis confirms that both Zn and Te elements are successfully deposited on the CdS:Ga NW surface (Fig. 1(f)). The doped Sb atoms cannot be distinguished due to the low doping concentration.

The chemical composition of the core–shell nanostructures was also confirmed by the XRD analysis. As shown in Fig. 2, all diffraction peaks in the pattern of CdS:Ga–ZnTe:Sb core–shell nanostructures can be indexed to hexagonal wurtzite phase CdS (JCPDS 41-1049),[31] and face-centered cubic ZnTe (JCPDS 15-0746).[32] Moreover, there are no other diffraction peaks from the impurities or contaminants, revealing the high crystalline purity of the product. Fig. 3(a) and (b) shows the XPS spectra of pure CdS:Ga and CdS:Ga–ZnTe:Sb core–shell nanostructures. Obvious peaks due to O, C, Cd, S, and Ga were observed in the pure CdS:Ga NW sample. The signal attributable to O and C is understandably due to surface absorption. Further XPS analysis reveals that once ZnTe:Sb was coated on the NWs, the signal ascribable to Ga, Cd and S all disappear (Fig. 3(b)), suggesting that the CdS:Ga NW has been completely wrapped by the ZnTe:Sb sheath.

Detailed microstructures of the CdS:Ga NWs and CdS:Ga–ZnTe:Sb core–shell NSs were then studied. Fig. 4(a) shows a typical TEM image of CdS:Ga–ZnTe:Sb core–shell NSs, the sharp distinction in contrast along the radial direction of the NS clearly reveals its core–shell structure. Fig. 4(b) shows a typical high resolution TEM (HRTEM) image of the CdS:Ga NW.

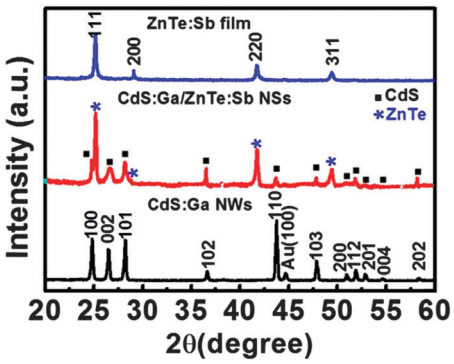

Fig. 2 XRD patterns of the CdS:GaNWs, CdS:Ga–ZnTe:Sb core–shell nanostructures, and pure ZnTe:Sb film.

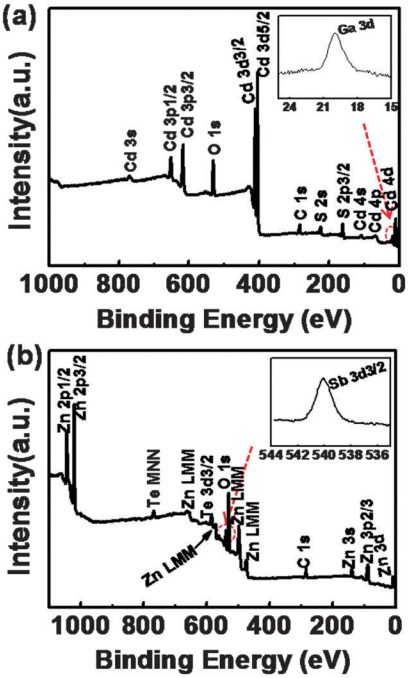

Fig. 3 (a) XPS survey spectrum of CdS:Ga NWs; the inset shows the Ga 3d spectrum. (b) XPS survey spectrum of CdS:Ga–ZnTe:Sb core–shell NSs; the inset shows the spectra of Sb 3d 3/2.

The lattice spacings of 0.36 nm and 0.68 nm correspond to the (100) and (001) plane of hexagonal CdS, in good agreement with the fast Fourier transform (FFT) pattern of the CdS NW (Fig. 4(c)). In addition, it can also be seen that the crystalline quality and structural integrity of CdS NWs are not degraded by gallium corporation. Fig. 4(d) shows a HRTEM image of the CdS–ZnTe core–shell NSs, which reveals that the ZnTe shell is composed of a large number of crystal grains with a nanoscale size of ~5–10 nm. The lattice spacings of the ZnTe shell are 0.21 nm, 0.35 nm and 0.61 nm, corresponding to the (220), (111) and (100) planes, respectively. The elemental mapping in Fig. 4(f)–(i) clearly displayed the spatial distributions of S, Cd, Te and Zn in the core and the shell. It shows that the ZnTe shell layer continuously covered the entire surface of the CdSNW core.

Although the doping concentrations of both Ga and Sb atoms are lower than the resolution of EDS (Fig. 1(e) and (f)), the electrical conductivity of the resultant NS is very high according to our electrical analysis. The black curve in Fig. 5(a) shows the *I–V* curves of an individual Ga doped CdS NW. The linear curves indicate good Ohmic contact between the electrodes and the samples. The current is as high as 50 μA at a bias voltage of 5 V. What is more, the conductivity is estimated to be 2.1×10^{-3} S cm^{-1}, much higher than that of intrinsic CdS, which is virtually insulating without impurity doping.[33] Fig. 5(b) shows the gate-dependent source–drain current (I_{DS}) *versus* voltage (V_{DS}) curves of an individual CdS:GaNW based FET. Obviously, the device showed a pronounced gating effect and I_{DS} increases with increasing V_G, indicative of typical behavior of an *n*-channel FET. The electronic carrier concentration and mobility of the CdS:GaNW core can be deduced to be

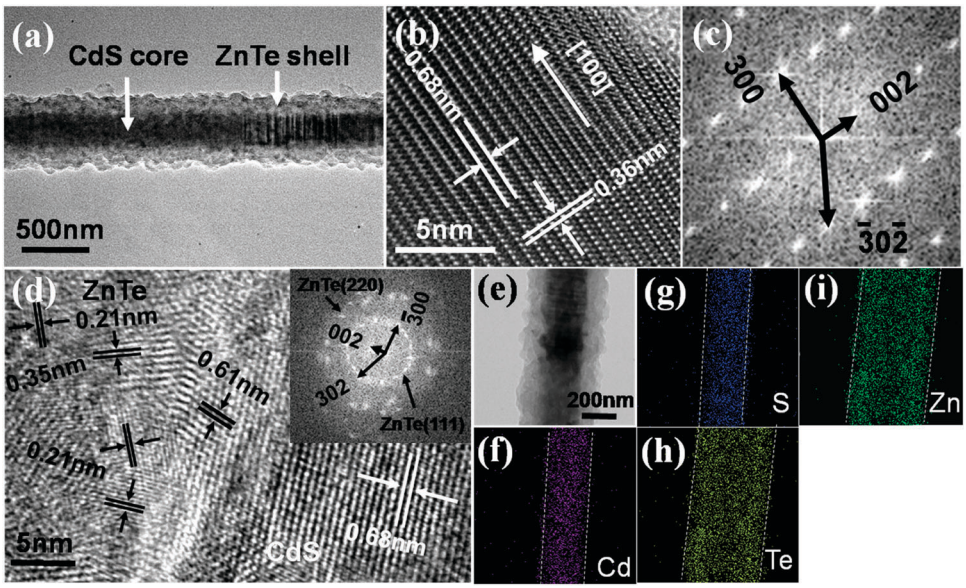

Fig. 4 (a) TEM image of a CdS:Ga–ZnTe:Sb core–shell NS. (b) HRTEM image of the CdS:GaNW, and (c) the corresponding FFT pattern. (d) High magnification TEM image of a CdS:Ga–ZnTe:Sb core–shell NS. (e–i) TEM image of an individual core–shell nanostructure and the corresponding elemental mapping images for Cd (f), S (g), Te (h) and Zn (i).

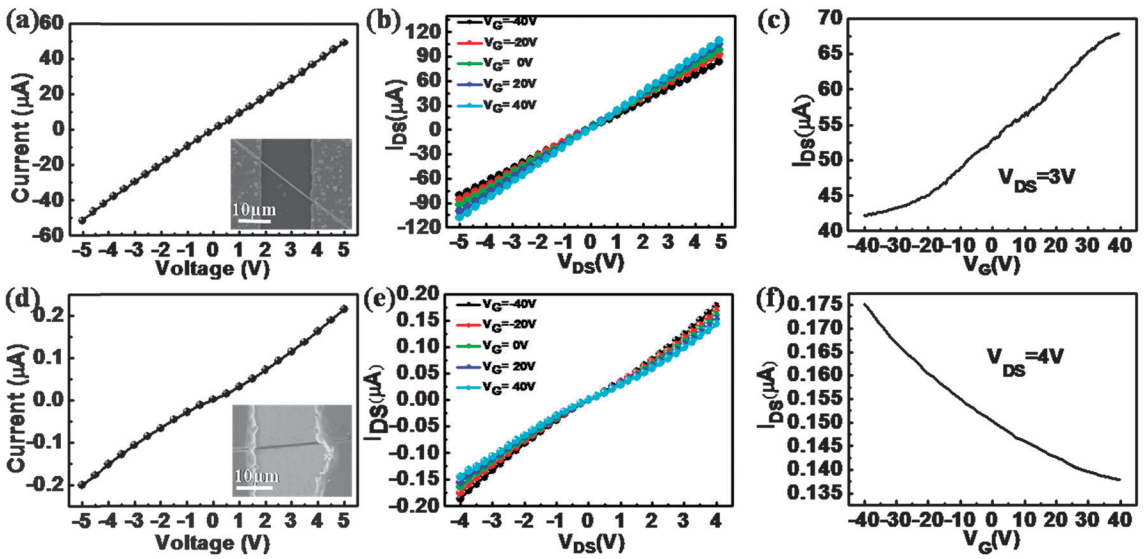

Fig. 5 (a) I–V curves of the CdS:Ga NW; the inset shows the corresponding SEM image of the nano-FET. (b) Electrical transport characteristics of the nano-FET fabricated from the CdS:Ga NW, (c) the I_{DS}–V_G curves measured at a V_{DS} of 3 V. (d) Typical I–V curves of the ZnTe:Sb shell; the inset shows the SEM image of the nano-FET. (e) Electrical transport characteristics of the Nano-FET fabricated from ZnTe:Sb shells, (f) the I_{DS}–V_G curves measured at a fixed V_{DS} of 4 V.

7.62×10^{17} cm^{-3} and 1.72×10^{-2} cm^2 V^{-1} s^{-1} respectively, consistent with literature values.[34,35] Unlike the CdS:Ga NW, the FET device assembled from the CdS:Ga–ZnTe:Sb NW exhibited obvious p-type conduction characteristic. That is, the I_{DS} increases with decreasing V_G (Fig. 5(d)). Understandably, such a p-type electrical characteristic is due to the ZnTe:Sb shell. In this case, the hole mobility and concentration are estimated to be 0.12 cm^2 V^{-1} s^{-1} and 1.3×10^{17} cm^{-3}, respectively.

Next, the optical properties of both CdS:GaNWs, ZnTe:Sb film, ZnTe:Sb film and core–shell CdS:Ga–ZnTe:SbNSs were investigated. Fig. 6(a) plots the absorption curves of the three samples, and it is clear that the exterior coating of the ZnTe:Sb sheath on CdS:GaNWs has an obvious effect on the optical properties of light absorption. The absorption edge red shifts from ~520 nm for CdS:GaNWs, to about 580 nm for the CdS:Ga–ZnTe:Sb core–shell NSs. For a direct bandgap semiconductor, the optical absorption near the band edge can be described by the equation of $\alpha h\nu = A(h\nu - E_g)^{1/2}$, where α, ν, E_g, and A are the absorption coefficient, the light frequency, the band gap energy of the semiconductor, and a constant, respectively.

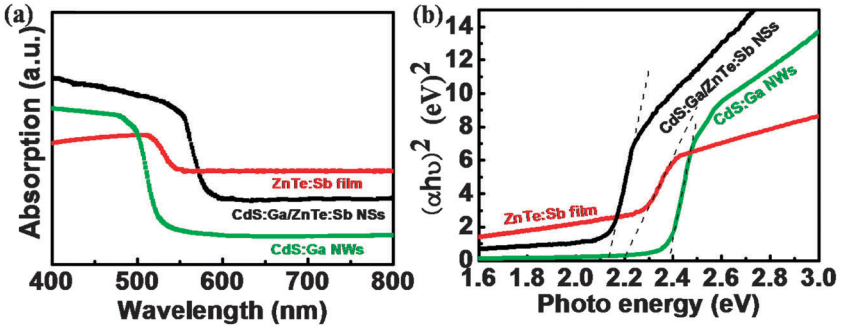

Fig. 6 UV-visible absorption spectra (a) and plots of $(\alpha h\nu)^2$ *vs.* photon energy ($h\nu$), (b) of CdS:GaNWs, CdS:Ga–ZnTe:Sb core–shell NSs, and ZnTe:Sb film at room temperature.

By extrapolating the curve in Fig. 6(b), the band-gaps of CdS ($E_{g,CdS}$) and ZnTe ($E_{g,ZnTe}$) are estimated to be 2.38 eV and 2.20 eV, respectively, consistent with literature values.[36,37] What is more, by using the same method, the E_g value for CdS:Ga–ZnTe:Sb NSs is deduced to be 2.13 eV, which is a little bit smaller than the E_g of ZnTe film. This is probably caused by the formation of the $Cd_{1-x}Zn_xTe$ phase and the coupling effect of ZnTe film.[38,39]

In order to explore the potential of the present NS for optoelectronic device application, a visible light photodetector was fabricated based on the nano-heterojunction. The detailed stepwise process for the fabrication of the device is illustrated in Fig. 7(a). Fig. 7(b) shows a representative FESEM image of the p–n junction device assembled from a single CdS:Ga–ZnTe:Sb core–shell NS. From the typical *I–V* characteristics of the CdS:Ga–ZnTe:Sb p–n junction measured in the dark and light in Fig. 7(d), one can see that the p–n junctions revealed excellent rectification behavior in the dark with a rectification ratio about 10^2 within ±1 V. For small forward bias, the junction

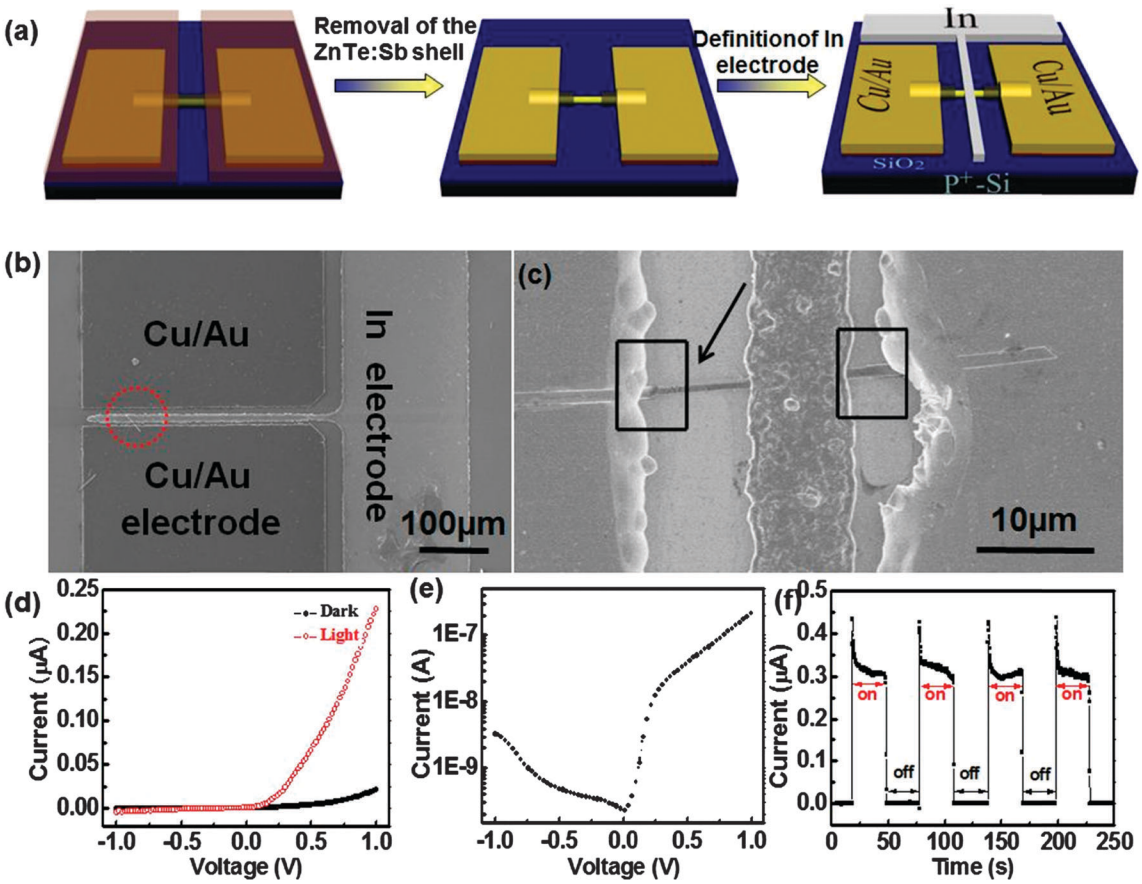

Fig. 7 (a) Stepwise process for the fabrication of a single CdS:Ga–ZnTe:Sb NS. (b and c) Representative FESEM images of a p–n junction device. (d) Rectification characteristics of the p–n junction measured both in the dark and under light illumination. (e) *I–V* curve of the p–n junction under light illumination at a log scale. (f) Photoresponse of the CdS:Ga–ZnTe:Sb NS to the pulsed light illumination, and the bias voltage is 1 V.

Table 1 Summary of the device performance of the CdS:Ga–ZnTe:Sb core–shell NS device with other detectors with similar device structures

Materials	R/A W^{-1}	G	D^*/cm Hz$^{1/2}$ W^{-1}	Ref.
CdS:Ga–ZnTe:SbNS	1.55×10^3	3.0×10^3	8.7×10^{12}	Our work
Arrays of CdS NWs	—	—	3×10^{11}	42
CdS QDs	—	—	1.37×10^8	43
Si–CdS NW	1.37	—	4.39×10^{11}	44
CdSe–CdS NSs	260	—	$>1 \times 10^{13}$	45

current (I) follows an exponential dependence on the applied bias (V), $I = I_0\left(\exp\left(\frac{eV}{nk_BT}\right) - 1\right)$, where I_0 is the reverse bias saturation current, e is the electron charge, k_B is the Boltzmann constant, T is the temperature, and n is the ideality factor. Based on this equation, the ideality factor is estimated to be 1.28, suggesting that the transport through the p–n junction may be due to thermionic emission.[40] Fig. 7(f) depicts the time response spectra of the p–n junction measured under light illumination with a wavelength of 638 nm (light intensity: 2 mW cm^{-2}) at 1 V. It shows excellent stability and reproducibility with a fast response time of less than 1 s. In addition, the I_{light}/I_{dark} ratio is estimated to be 20.

To further evaluate the optoelectronic characteristics of the CdS:Ga–ZnTe:Sb core–shell NS, we measured their responsivity R (A W^{-1}), conductive gain G and detectivity D^* (cm Hz$^{1/2}$ W^{-1}), which can be expressed by using eqn (1) and (2),[41] respectively:

$$R(\text{A W}^{-1}) = \left(\frac{I_p}{P_{opt}}\right) = \eta\left(\frac{q\lambda}{hc}\right)G \quad (1)$$

$$D^* = A^{1/2}R/(2qI_d)^{1/2} = A^{1/2}(I_p/I_{opt})/(2qI_d)^{1/2} \quad (2)$$

where I_p is the photocurrent, P_{opt} the incident light power, η the quantum efficiency, λ the light wavelength, h the Planck's constant, c the speed of light and G the photoconductive gain. The values of P_{opt}, q, λ, h, and c are 2 mW cm^{-2}, 1.6×10^{-19} C, 638 nm, 6.625×10^{-34} J s and 3×10^8 m s^{-1}, respectively. By assuming η = 1 for simplification, the responsivity (R) and detectivity (D^*) are estimated to be 1.55×10^3 A W^{-1} and 8.7×10^{12} cm Hz$^{1/2}$ W^{-1} for the CdS:Ga–ZnTe:Sb core–shell NS at a bias voltage of 1 V, respectively. Table 1 compares the performance of our device with that of other similar devices. It is visible that although the detectivity is slightly poorer than that of CdSe/CdS NSs,[45] but the responsivity, gain and detectivity are much higher than the devices based on arrays of CdS NWs,[42] CdS QDs,[43] Si–CdS core–shell NWs,[44] suggesting that the present device will have great potential for future optoelectronic device application.

Conclusions

In conclusion, we have synthesized high-quality CdS:Ga–ZnTe:Sb core–shell NSs on a silicon substrate by using a two-step CVD method. The ZnTe shell is uniformly deposited on the entire surface of the CdS:Ga NWs along the whole length to form the core–shell NSs. The light absorption range of the CdS:Ga–ZnTe:Sb core–shell NSs is wider than that of CdS:Ga NWs. Moreover, the core–shell p–n junction devices exhibit excellent rectifying characteristics with a low turn-on voltage of ~0.25 V, a rectification ratio of ~10^2, and an ideality factor of 1.28. In addition, the CdS:Ga–ZnTe:Sb core–shell NS exhibits obvious sensitivity to 638 nm light irradiation, and the corresponding I_{light}/I_{dark} ratio is estimated to be 20. We believe the present one-dimensional core–shell hetero-junction will have great potential for future optoelectronic device application.

Acknowledgements

This work was supported by the financial support from the China Scholarship Council, the Natural Science Foundation of China (No. 61106010, 21101051, and 21301044), the Natural Science Foundation of Anhui Province (Grant No. J2014AKZR0059), and the Fundamental Research Funds for the Central Universities (No. 2012HGCX0003, 2013HGXJ0195, 2013HGCH0012, and 2014HGCH0005).

References

1 J. S. Jie, W. J. Zhang, I. Bello, C. S. Lee and S. T. Lee, *Nano Today*, 2010, **5**, 313.
2 B. Nie, J. G. Hu, L. B. Luo, C. Xie, L. H. Zeng, P. Lv, F. Z. Li, J. S. Jie, M. Feng, C. Y. Wu, Y. Q. Yu and S. H. Yu, *Small*, 2013, **9**, 2872.
3 Z. L. Wang and J. H. Song, *Science*, 2006, **312**, 5771.
4 C. Soci, A. Zhang, B. Xiang, S. A. Dayeh, D. P. R. Aplin, J. Park, X. Y. Bao, Y. H. Lo and D. Wang, *Nano Lett.*, 2007, **7**, 1003.
5 J. X. Wang, C. Y. Yan, M. F. Lin, K. Tsukagoshi and P. S. Lee, *J. Mater. Chem. C*, 2015, **3**, 596.
6 J. Debgupta, R. Devarapalli, S. Rahman, M. V. Shelke and V. K. Pillai, *Nanoscale*, 2014, **6**, 9148.
7 B. Hua, J. Motohisa, Y. Kobayashi, S. Hara and T. Fukui, *Nano Lett.*, 2009, **9**, 112.
8 Y. Tak, S. J. Hong, J. S. Lee and K. Yong, *J. Mater. Chem.*, 2009, **19**, 5945.
9 Z. M. Wu, Y. Zhang, J. J. Zheng, X. G. Lin, X. H. Chen, B. W. Huang, H. Q. Wang, K. Huang, S. P. Li and J. Y. Kang, *J. Mater. Chem.*, 2011, **21**, 6020.
10 J. Y. Huang, S. Liu, Y. Wang and Z. Z. Ye, *Appl. Surf. Sci.*, 2008, **254**, 5917.
11 S. H. Shin, M. H. Lee, J. Y. Jung, J. H. Seol and J. Nah, *J. Mater. Chem. C*, 2015, **3**, 8103.
12 Z. J. Li, Z. P. Hu, J. Peng, C. Z. Wu, Y. C. Yang, F. Feng, P. Gao, J. L. Yang and Y. Xie, *Adv. Funct. Mater.*, 2014, **24**, 1821.
13 B. N. Pal, Y. Ghosh, S. Brovelli, R. Laocharoensuk, V. I. Klimov, J. A. Hollingsworth and H. Htoon, *Nano Lett.*, 2012, **12**, 331.
14 G. Schmuelling, N. Oehl, M. Knipper, J. Kolny-Olesiak, T. Plaggenborg, H. W. Meyer, T. Placke, J. Parisi and M. Winter, *Nanotechnology*, 2014, **25**, 35.

15 Z. P. Sun, W. Ai, J. L. Liu, X. Y. Qi, Y. L. Wang, J. H. Zhu, H. Zhang and T. Yu, *Nanoscale*, 2014, **6**, 6563.
16 G. H. Li, Y. Jiang, Y. G. Zhang, X. Z. Zhang, T. Y. Zhai and G. C. Yi, *J. Mater. Chem. C*, 2014, **2**, 8252.
17 A. L. Pan, R. B. Liu, M. H. Sun and C. Z. Ning, *ACS Nano*, 2010, **4**, 671.
18 S. Kellar, C. Ballal, A. Deshpanda, S. Warule and S. Ogale, *J. Mater. Chem. A*, 2013, **1**, 12426.
19 J. S. Jie, W. J. Zhang, Y. Jiang and S. T. Lee, *Appl. Phys. Lett.*, 2006, **89**, 223117.
20 L. Wang, X. A. Wang, R. Chen, C. Y. Wu, Y. Q. Yu, J. Xu, J. G. Hu and L. B. Luo, *J. Appl. Phys.*, 2014, **115**, 063108.
21 F. Z. Li, L. B. Luo, Q. D. Yang, D. Wu, C. Xie, B. Nie, J. S. Jie, C. Y. Wu, L. Wang and S. H. Yu, *Adv. Energy Mater.*, 2013, **3**, 579.
22 Y. Ye, Y. Dai, L. Dai, Z. J. Shi, N. Liu, F. Wang, L. Fu, R. M. Peng, X. N. Wen and Z. J. Chen, *ACS Appl. Mater. Interfaces*, 2010, **2**, 3406.
23 Y. Xiao, C. Meng, P. Wang, Y. Ye, H. K. Yu, S. S. Wang, F. X. Gu, L. Dai and L. M. Tong, *Nano Lett.*, 2011, **11**, 1122.
24 J. A. Zapien, Y. K. Liu, Y. Y. Shan, H. Tang, C. S. Lee and S. T. Lee, *Appl. Phys. Lett.*, 2007, **90**, 213114.
25 J. Y. Xu, X. J. Zhuang, P. F. Guo, Q. L. Zhang, W. Q. Huang, Q. Wan, W. Hu, X. X. Wang, X. L. Zhu, C. Z. Fan, Z. Y. Yang, L. M. Tong, X. F. Duan and A. L. Pan, *Nano Lett.*, 2012, **12**, 5003.
26 R. M. Ma, L. Dai, H. B. Huo, W. J. Xu and G. G. Qin, *Nano Lett.*, 2007, **7**, 3300.
27 J. S. Jie, W. J. Zhang, Y. Jiang, X. M. Meng, Y. Q. Li and S. T. Lee, *Nano Lett.*, 2006, **6**, 1887.
28 D. Wu, Y. Jiang, Y. G. Zhang, Y. Q. Yu, Z. F. Zhu, X. Z. Lan, C. Y. Wu, L. Wang and L. B. Luo, *J. Mater. Chem.*, 2012, **22**, 23272.
29 T. Dietl, H. Ohno, F. Matsukura, J. Cibert and D. Ferrand, *Science*, 2000, **287**, 1019.
30 L. B. Luo, S. H. Zhang, R. Lu, W. Sun, Q. L. Fang, C. Y. Wu, J. G. Hu and L. Wang, *RSC Adv.*, 2015, **5**, 13324.
31 J. H. Zhan, X. G. Yang, D. W. Wang, S. D. Li, Y. Xie, Y. N. Xia and Y. T. Qian, *Adv. Mater.*, 2000, **12**, 1348.
32 Y. L. Cao, Z. T. Liu, L. M. Chen, Y. B. Tang, L. B. Luo, J. S. Jie, W. J. Zhang, S. T. Lee and C. S. Lee, *Opt. Express*, 2011, **19**, 6100.
33 D. Wu, Y. Jiang, L. Wang, S. Y. Li, B. Wu, Y. Q. Yu, C. Y. Wu and J. S. Jie, *Appl. Phys. Lett.*, 2010, **96**, 123118.
34 C. Y. Wu, J. S. Jie, L. Wang, Y. Q. Yu, Q. Peng, X. W. Zhang, J. J. Cai, H. E. Guo, D. Wu and Y. Jiang, *Nanotechnology*, 2010, **21**, 505203.
35 J. J. Cai, J. S. Jie, P. Jiang, D. Wu, C. Xie, C. Y. Wu, Z. Wang, Y. Q. Yu, L. Wang and X. W. Zhang, *Phys. Chem. Chem. Phys.*, 2011, **13**, 14663.
36 L. Li, P. C. Wu, X. S. Fang, T. Y. Zhai, L. Dai, M. Y. Liao, Y. Koide, H. Q. Wang, Y. Bando and D. Golberg, *Adv. Mater.*, 2010, **22**, 3161.
37 M. F. Ehsan, M. N. Ashiq and T. He, *RSC Adv.*, 2015, **5**, 6186.
38 K. Wang, S. C. Rai, J. Marmon, J. J. Chen, K. Yao, S. Wozny, B. B. Cao, Y. F. Yan, Y. Zhang and W. L. Zhou, *Nanoscale*, 2014, **6**, 3679.
39 S. P. Tobin, J. P. Tower, P. W. Norton, D. Chandlerhorowitz, P. M. Amirtharaj, V. C. Lopes, W. M. Duncan, A. J. Syllaios, C. K. Ard, N. C. Giles, J. Lee, R. Balasubramanian, A. B. Bollong, T. W. Steiner, M. L. W. Thewalt, D. K. Bowen and B. K. Tanner, *J. Electron. Mater.*, 1995, **24**, 697.
40 M. Z. Wang, F. X. Liang, B. Nie, L. H. Zeng, L. X. Zheng, P. Lv, Y. Q. Yu, C. Xie, Y. Y. Li and L. B. Luo, *Part. Part. Syst. Charact.*, 2013, **30**, 630.
41 L. H. Zeng, M. Z. Wang, H. Hu, B. Nie, Y. Q. Yu, C. Y. Wu, L. Wang, J. G. Hu, C. Xie, F. X. Liang and L. B. Luo, *ACS Appl. Mater. Interfaces*, 2013, **5**, 9362.
42 F. F. Amos, S. A. Morin, J. A. Streifer, R. J. Hamers and S. Jin, *J. Am. Chem. Soc.*, 2007, **129**(36), 14296.
43 J. G. He, J. J. Chen, Y. Yu, L. Zhang, G. Z. Zhang, S. L. Jiang, W. Liu, H. S. Song and J. Tang, *J. Mater. Sci.*, 2014, **25**, 1499.
44 S. Manna, S. Das, S. P. Mondal, R. Singha and S. K. Ray, *J. Phys. Chem. C*, 2012, **116**, 7126.
45 J. S. Lee, M. V. Kovalenko, J. Huang, D. S. Chung and D. V. Talapin, *Nat. Nanotechnol.*, 2011, **6**, 348.